

Electroweak sphalerons, scalar multiplets, and symmetry breaking patterns

Yanda Wu,^{1,2,*} Wenxing Zhang,^{1,2,†} and Michael J. Ramsey-Musolf^{1,2,3,4,‡}

¹*Tsung-Dao Lee Institute and School of Physics and Astronomy,
Shanghai Jiao Tong University, 800 Dongchuan Road, Shanghai, 200240 China*

²*Shanghai Key Laboratory for Particle Physics and Cosmology,
Key Laboratory for Particle Astrophysics and Cosmology (MOE),
Shanghai Jiao Tong University, Shanghai 200240, China*

³*Amherst Center for Fundamental Interactions, Department of Physics,
University of Massachusetts Amherst, MA 01003, USA*

⁴*Kellogg Radiation Laboratory, California Institute of Technology, Pasadena, CA 91125 USA*

(Dated: July 6, 2023)

In this study, we present a comprehensive analysis of the electroweak sphaleron formalism and its application to electroweak phase transition (EWPT) patterns in extensions of the Standard Model scalar sector with electroweak multiplets. We offer an equivalence proof for different choices for the form of sphaleron configurations; construct the previously unestablished high-dimensional SU(2) sphaleron transformation matrix; and revisit the required boundary conditions needed for solving the sphaleron field equations. We then investigate the leading order sphaleron dynamics in the context of a multi-step EWPT. We showcase two distinct analytical approaches for extending the SU(2) scalar multiplet to the standard model (SM) under differing EWPT scenarios, and perform an explicit calculation of the sphaleron energy using a septuplet example. In the context of a single-step EWPT leading to a mixed phase, we find that the additional multiplet's contribution to the sphaleron energy is negligible, primarily due to the prevailing constraint imposed by the ρ parameter. Conversely, in a two-step EWPT scenario, the sphaleron energy can achieve significantly high values during the initial phase, thereby markedly preserving baryon asymmetry if the universe undergoes a first-order EWPT. In both cases, we delineate the relationship between the sphaleron energy and the parameters relevant to dark matter phenomenology.

PACS numbers:

I. INTRODUCTION

The origin of Baryon Asymmetry of the Universe (BAU) remains an open question in the frontier of particle physics and cosmology. In order to explain the BAU, Sakharov proposes three necessary conditions: (1) baryon-number violation; (2) C and CP violation; (3) departure from thermal equilibrium or CPT violation [1]. In principle, the Standard Model (SM) provides all the necessary ingredients for generation of the baryon asymmetry during the era of electroweak symmetry-breaking (EWSB), a scenario known as electroweak baryogenesis (EWBG). Indeed, the first condition can be fulfilled by the non-perturbative weak sphaleron process. However, the SM fails to satisfy the second and third conditions. The CP-violation associated with the Cabibbo-Kobayashi-Maskawa matrix is too weak to generate the observed BAU [2–4], and EWSB occurs through a smooth crossover transition due to the large Higgs mass [5–9], thereby missing the needed out of equilibrium requirement. Many beyond Standard Model (BSM) theories have been proposed to remedy these shortcomings and facilitate EWBG (please see [10, 11] for reviews). In this

work, we focus on a key element of BSM EWBG: electroweak sphaleron dynamics. We do so in the context of a general class of BSM scenarios, namely, those involving an extended Higgs sector containing higher dimensional electroweak multiplets.

Electroweak baryogenesis requires a first order electroweak phase transition (FOEWPT), during which bubbles of broken symmetry nucleate in the symmetric phase. The BSM CP-violating interactions at the bubble walls generate a left-handed fermion number density that biases symmetric phase sphaleron transitions into generation of non-zero baryon plus lepton number ($B + L$) [10, 12, 13]. The asymmetry diffuses into the bubble interiors. A sufficiently “strong” FOEWPT leads to suppression of the broken phase sphaleron rate, thereby allowing preservation of the asymmetry [14]. A central question, therefore, pertains to the broken phase sphaleron rate: is it sufficiently quenched so as to preserve the BAU?

While the most reliable approaches to answering this question are obtained using lattice computations, as a practical matter performing a broad survey of BSM scenarios and associated parameter choices relies on (semi-)analytic methods and perturbation theory. The latter provides a baseline for comparison and validation against non-perturbative studies. The aim of the following study is to refine this baseline and clarify some formal considerations along the way. In doing so, we recall that the analytic result for the broken phase sphaleron rate, Γ_{WS} can be written as the product of a dynamical prefactor

*Electronic address: yanda.wu7@sjtu.edu.cn

†Electronic address: zhangwenxing@sjtu.edu.cn

‡Electronic address: mjrm@sjtu.edu.cn, mjrm@physics.umass.edu

A and a statistical factor [15–17]:

$$\Gamma_{\text{WS}} = A e^{-E_{\text{sph}}/T} \quad , \quad (1)$$

where E_{sph} is the energy associated with the semiclassical sphaleron solution. Our focus in the present study falls on the latter.

To further set the context, we recall that the thermal history of EWSB can entail either a single, direct transition to the present ‘‘Higgs phase’’ or a series of steps. In the presence of additional scalar fields Φ , a different vacuum associated with a non-zero vacuum expectation value (vev) for one or more components of Φ may precede the Higgs phase. Alternately, the Higgs phase may also involve a non-zero Φ vev. While Φ may be either a SM gauge singlet or carry SM quantum numbers, in this study we consider the case where Φ is an $SU(3)_C$ singlet but charged under $SU(2)_L \times U(1)_Y$. We further specify that only the neutral component of Φ obtains a non-zero vev. Three representative patterns of EWSB are illustrated in Figure 1, where case (a), (b) and (c) represent the SM one-step EWPT, one-step EWPT to the mixed phase and two-step EWPT, respectively.

Each case may accommodate EWBG. For the single-step transitions in (a) and (b), the presence of Φ will modify Γ_{WS} through thermal loops and, for (b), through additional contributions to the semiclassical sphaleron solution. Note that for (b), constraints from the electroweak ρ -parameter place strong constraints on $\langle \Phi \rangle$, when Φ is neither a gauge singlet or second Higgs doublet. One may evade these constraints through a suitable choice of field content, as in the Georgi-Machacek model [18]. For (c), the first step may accommodate EWBG if (i) this step involves a FOEWPT; (ii) if BSM CPV interactions generate a sufficiently large asymmetry; (iii) Γ_{WS} in the EWSB Φ vacuum is sufficiently suppressed; and (iv) the second step to the Higgs phase does not allow for re-excitation of the EW sphalerons. The viability of this possibility has been demonstrated in Refs. [19–21]. To our knowledge, EW sphaleron dynamics for these scenarios in the presence of Φ have not been explored in a unified and systematic way. In what follows we endeavor to do so, focusing on cases (b) and (c) wherein Φ can play an active role in the semiclassical sphaleron solution. We investigate both the corresponding topological structure and sphaleron energy.

Thus, this study mainly consists of two parts. In the first part, we review, update, and clarify various formal aspects related to the semiclassical treatment of the sphaleron in BSM theories, including: relationships between various treatments for the sphaleron configuration; a general construction of the 1-form framework for a general scalar multiplet; restrictions arising in the presence of more than one scalar field multiplet; topology pertaining to higher dimensional (beyond doublet) multiplets; equation of motion and choice of boundary conditions. We intent our discussion of these issues to provide a general reader with some background as well as to set the context for our specific choices in the second part of the

study.

In the latter part, we compute the sphaleron energy for scenarios (b) and (c) for Φ being an electroweak septuplet, whose presence in the Higgs vacuum of scenario (c) can contribute to the dark matter (DM) relic density. In this instance, we delineate the dependence of E_{sph} on the parameters relevant to DM phenomenology: the DM mass, its self-interaction, and the coupling to SM fields that enters the annihilation and direct detection cross sections. In our current work, we primarily focus on the analysis of the zero-temperature model. Our aim is to provide a methodology for applying the sphaleron formalism to different EWSB patterns, where the zero-temperature model can provide a good approximation of physical quantities. The thermally corrected model can be analyzed in a parallel manner. We find that, depending on the values of these parameters, E_{sph} for step C1 of case (c) can be significantly larger than in the SM for single step transition in case (a), suggesting that the two-step scenario can be particularly conducive to EWBG.

Our discussion of these issues is organized as follows. In section II, we present a detailed analysis of the sphaleron formalism, either in SM or in BSM scenarios. In section III, we discuss an electroweak multiplet extension to the SM and present three possible types of EWPT after this extension. In section IV, we compute the sphaleron energy of this model under different types of EWPT.

II. SPHALERON FORMALISM

In this section, we address several issues pertaining to sphaleron formalism:

- We first summarize the most widely considered choices for the sphaleron configurations and construct the relations between them, starting with the Weinberg-Salam theory.
- As we will utilize the 1-form choice when treating higher dimensional multiplets, we give a general construction in terms of Wigner D-matrices that applies to scalar fields of arbitrary isospin.
- We apply this construction to an extended scalar sector and point out restrictions on the scalar potential needed to accommodate a multi-scalar field sphaleron solution.
- For Φ differing from a scalar doublet, we demonstrate the dependence of the sphaleron solution on additional multiplet to ensure the sphaleron solution yields the baryon plus lepton charge $Q_{B+L} = 1$ (equivalent to $Q_B = 1/2$ since $B - L$ is conserved by the sphaleron transitions) .
- We review the derivation of the sphaleron field equations for a general electroweak multiplet and clarify requirements on the corresponding boundary conditions.

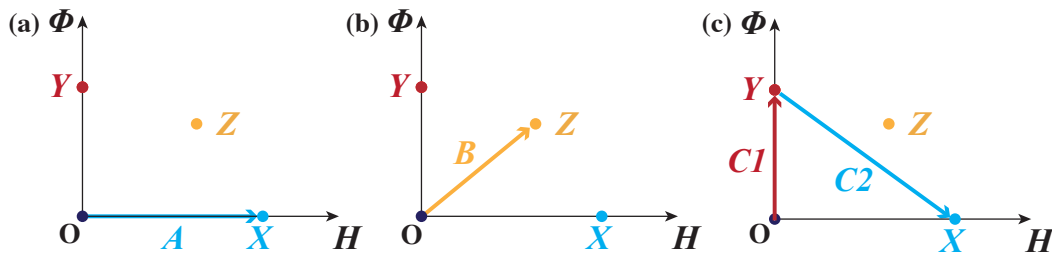


Figure 1: Three possible EWSB patterns. In each plot, the horizontal axis represents the SM Higgs vacuum, the vertical axis stands for the BSM (electroweak multiplet in our study) particle's vacuum. The O denotes the symmetric phase, while X , Y and Z represent three saddle points of the total potential. (a) represents a one-step EWPT from symmetric phase to pure Higgs phase; (b) denotes a one-step EWPT to the mixed phase where the Higgs particle and scalar multiplet particle both obtain a vacuum expectation value (vev); (c) depicts a two-step EWPT scenario, where the first step moves from symmetric phase to the pure multiplet phase, and the second step moves from the multiplet phase to the Higgs phase.

A. Sphaleron configurations in the Standard Model

The SM electroweak sphaleron formalism is first constructed by Manton and Klinkhamer [22, 23]. Klinkhamer and Laterveer later propose another sphaleron configuration with a different field configuration from Manton and Klinkhamer's one [24]. We will demonstrate that these two configurations are equivalent to each other under a sphaleron gauge transformation. Other sphaleron configurations are also been discussed in this work, like Refs. [25–27].

Manton first constructs the sphaleron topological non-contractible loop (NCL) within the Weinberg-Salam theory. Through the topological identity map, the Higgs field at spatial infinity is parameterized as [22]

$$H^\infty(\mu, \theta, \phi) = \begin{bmatrix} H_1^\infty \\ H_2^\infty \end{bmatrix} = \begin{bmatrix} \sin \mu \sin \theta e^{i\phi} \\ e^{-i\mu} (\cos \mu + i \sin \mu \cos \theta) \end{bmatrix}, \quad (2)$$

where the Higgs field at spatial infinity $r \rightarrow \infty$ is denoted as H^∞ . The parameter $\mu \in [0, \pi]$ characterizes motion along the NCL, where $\mu = 0, \pi$ correspond to vacuum and $\mu = \frac{\pi}{2}$ corresponds the sphaleron configuration. Other two parameters θ and ϕ are two spherical angles at spatial infinity. The unitary transformation matrix U^∞ is constructed as

$$U^\infty = \begin{bmatrix} H_2^{\infty*} & H_1^\infty \\ -H_1^{\infty*} & H_2^\infty \end{bmatrix}, \quad (3)$$

Then the field configurations for arbitrary r are given in [23]

$$H(\mu, \xi, \theta, \phi) = \frac{v}{\sqrt{2}} h(\xi) U^\infty \begin{pmatrix} 0 \\ 1 \end{pmatrix}, \quad (4)$$

$$\mathbf{A}_i(\mu, \xi, \theta, \phi) dx^i = -\frac{i}{g} f(\xi) \partial_i U^\infty (U^\infty)^{-1}.$$

where $\xi = g\Omega r$ is a dimensionless radial parameter with $\Omega = 246.22$ GeV; v is the Higgs vev; $\mathbf{A}_i = A_i^a \sigma^a / 2$, where σ^a denotes the Pauli matrix; and g represents the weak

gauge coupling constant. Under the spherical symmetry ansatz, $h(\xi)$ and $f(\xi)$ denote the Higgs field and gauge field radial profile function. The radial profile functions satisfy a set of coupled differential equations implied by the field's Euler-Lagrangian equation, whose boundary conditions will be discussed in later subsection. Note that $i \in [r, \theta, \phi]$ in spherical coordinate. Since the radial gauge is applied, the radial component of the gauge field A_r^a vanishes.

Klinkhamer and Laterveer propose a different field configuration [24] (denoted here as the KL configuration), while their sphaleron matrix U^∞ is identical with Manton and Klinkhamer's original construction [23] (denoted as the MK configuration). The KL configuration defines the 1-form F_a via

$$i(U^{\infty-1})dU^\infty = \sum_{a=1}^3 F_a \frac{\sigma^a}{2}. \quad (5)$$

where the F_a are crucial for the sphaleron Yang-Mills and kinetic parts energy calculation.

The NCL in KL configuration commences and terminates at the topologically different vacua, and is composed of three phases [24]

- I, $\mu \in [-\pi/2, 0]$: builds up the Higgs field configuration;
- II, $\mu \in [0, \pi]$: builds up and destroys the gauge field configuration;
- III, $\mu \in [\pi, 3\pi/2]$: destroys the Higgs field configuration.

where $\mu = -\pi/2, 3\pi/2$ represent the vacuum configuration and $\mu = \pi/2$ denotes the sphaleron configuration. In different phases, the sphaleron's profile functions are different. In phase I and III, the profile function is given by

$$\mathbf{A}_i = a_i = 0,$$

$$H(\mu, \xi, \theta, \phi) = \frac{v (\sin^2 \mu + h(\xi) \cos^2 \mu)}{\sqrt{2}} \begin{pmatrix} 0 & 1 \end{pmatrix}^T, \quad (6)$$

where a_i denotes the $U(1)$ gauge field. While in phase II, the field configuration read

$$\begin{aligned} H(\mu, \xi, \theta, \phi) &= \frac{v}{\sqrt{2}} h(\xi) \begin{pmatrix} 0 \\ 1 \end{pmatrix}, \\ \mathbf{A}_i dx^i &= \frac{1}{g} (1 - f(\xi)) \left[F_1 \frac{\sigma_1}{2} + F_2 \frac{\sigma_2}{2} \right] \\ &\quad + \frac{1}{g} (1 - f_3(\xi)) \left[F_3 \frac{\sigma_3}{2} \right], \\ a_i dx^i &= (1 - f_0(\xi)) F_3. \end{aligned} \quad (7)$$

where a_i represents the $U(1)$ gauge field, and g' denotes the $U(1)$ gauge coupling constant.

We now show the equivalence of this KL field configuration with the MK configuration under the $f_0 = 0$ and $f = f_3$ restrictions. Apply an unitary transformation $(U^\infty)^{-1}$ to the MK configuration, eq. (4). The Higgs field becomes

$$H(\mu, \xi, \theta, \phi) \rightarrow \frac{v}{\sqrt{2}} h(\xi) \begin{pmatrix} 0 \\ 1 \end{pmatrix}, \quad (8)$$

The gauge field transforms in the usual way $\mathbf{A}_\mu \rightarrow U \mathbf{A}_\mu U^{-1} - \frac{i}{g} (\partial_\mu U) U^{-1}$, so the transformed gauge field becomes

$$\begin{aligned} \mathbf{A}_i dx^i &\rightarrow (U^\infty)^{-1} \left(-\frac{i}{g} f(\xi) \partial_i U^\infty (U^\infty)^{-1} \right) U^\infty \\ &\quad - \frac{i}{g} \partial_i (U^\infty)^{-1} U^\infty \\ &= \frac{i}{g} (1 - f(\xi)) (U^\infty)^{-1} \partial_i U^\infty \\ &= \frac{1}{g} (1 - f(\xi)) \left[F_1 \frac{\sigma_1}{2} + F_2 \frac{\sigma_2}{2} + F_3 \frac{\sigma_3}{2} \right]. \end{aligned} \quad (9)$$

Under the symmetric ansatz ($f = f_3, f_0 = 1$), the Higgs field and non-abelian gauge field configurations in eq. (7) are equal to the gauge transformed configurations eq. (8) and eq. (9). Hence, the MK configuration is a special (zero mixing angle) case of KL configuration with the additional stipulation $f = f_3$.

Different gauge field configurations should lead to the same sphaleron energy, which is gauge independent. Apart from the MK and KL configurations, there are other sphaleron configurations. Akiba, Kikuchi and Yanagida propose the field configuration from the general spherical symmetric ansatz [25], denoted here as the AKY configuration. Kleihaus, Kunz and Brihaye construct the configuration based on a set of orthonormal vector [27], which is quite similar with Rebbi and Rossi' monopole solution [26], and we will name this as KKB configuration. To serve as a comprehensive summary of sphaleron configurations, we discuss the AKY and KKB configurations into the Appendix. AKY in [25] shows that their field solutions are totally equivalent with MK sphaleron configuration. Besides, the work [28] compares the MK and AKY configurations from the perspective of Bloch wave function.

In the remainder of this work, we will generalize the sphaleron configuration with scalar multiplet based on the KL configuration.

B. A general 1-form for $SU(2)$ multiplet

To that end, it is useful to provide a general construction of the 1-form F_a applicable to a general scalar $SU(2)_L$ multiplet of arbitrary isospin J . In passing, we note that Ahriche et al. [29] calculate the sphaleron energy for higher dimensional $SU(2)$ scalar representations, wherein they use but do not prove that the 1-form F_a is invariant property concerning different representation dimensions. We will expand on their work by showing this invariance.

An arbitrary $SU(2)$ matrix can be parameterized in terms of Wigner-D matrix, which in the fundamental representation reads

$$\begin{aligned} U(\alpha, \beta, \gamma) &= \mathcal{D}_{m, m'}^{1/2}(\alpha, \beta, \gamma) \\ &= e^{-i\alpha \frac{\sigma_3}{2}} e^{-i\beta \frac{\sigma_2}{2}} e^{-i\gamma \frac{\sigma_3}{2}} \\ &= \begin{pmatrix} e^{-i\frac{\alpha+\gamma}{2}} \cos \frac{\beta}{2} & -e^{-i\frac{\alpha-\gamma}{2}} \sin \frac{\beta}{2} \\ e^{i\frac{\alpha-\gamma}{2}} \sin \frac{\beta}{2} & e^{i\frac{\alpha+\gamma}{2}} \cos \frac{\beta}{2} \end{pmatrix}, \end{aligned} \quad (10)$$

where α, β, γ are three Euler angles. Comparing this matrix with sphaleron matrix eq. (3), we can obtain the following relationships

$$\begin{aligned} \cos \left(\frac{\beta}{2} \right) \cos \left(\frac{\alpha}{2} + \frac{\gamma}{2} \right) &= 1 + \sin^2 \mu (\cos \theta - 1), \\ \sin \left(\frac{\beta}{2} \right) \sin \left(\frac{\alpha}{2} - \frac{\gamma}{2} \right) &= \sin \phi \sin \theta \sin \mu, \\ \sin \left(\frac{\beta}{2} \right) \cos \left(\frac{\alpha}{2} - \frac{\gamma}{2} \right) &= -\cos \phi \sin \theta \sin \mu, \\ \cos \left(\frac{\beta}{2} \right) \sin \left(\frac{\alpha}{2} + \frac{\gamma}{2} \right) &= \sin \mu \cos \mu (\cos \theta - 1). \end{aligned} \quad (11)$$

we obtain these relations by (i) expand eq. (10) and eq. (3) into matrix addition with basis $I_{2 \times 2}, \sigma_1, \sigma_2$ and σ_3 ; (ii) equal the basis coefficients of these two matrices. While it is possible in principle to solve these equations and establish relationships between (α, β, γ) and (μ, θ, ϕ) , doing so in practice is cumbersome. Not only must we be careful with the sign of the final solution of three Euler angles, but also they have non-linear dependence with μ, θ, ϕ , complicating the calculation of the 1-form. Therefore, although eq. (10) looks quite intuitive, we seek an alternate method.

Instead, we can use the multiplication of multiple Wigner-D matrices to represent the sphaleron matrix. For a general representation J with matrix dimension $2J + 1$, we can write the sphaleron matrix as

$$U_{mn}^\infty(\mu, \theta, \phi) = \sum_{m'} D_{mm'}^J(\omega_-, -\theta, \mu) D_{m'n}^J(\mu, \theta, \omega_+), \quad (12)$$

with

$$\omega_{\pm} = -\mu \pm \left(\phi - \frac{\pi}{2}\right). \quad (13)$$

if we set $J = 1/2$, we can restore the standard sphaleron matrix eq. (3). This kind of parameterization method is quite easy to calculate the 1-form, since the Euler parameters are linear with respect to μ, θ and ϕ .

A general formation of F_a in the representation J can be calculated through the generalization of eq. (5)

$$i(U^{\infty-1})dU^{\infty} = \sum_{a=1}^3 F_a T_a, \quad (14)$$

where T_a are the $SU(2)$ generators in a general representation. The 1-form F_a can then be calculated through

$$F_3 = \frac{1}{\text{Tr}(T_3^2)} \text{Tr}[i(U^{\infty})^{-1}dU^{\infty}.T_3], \quad (15)$$

and

$$F_1 T_1 + F_2 T_2 = i(U^{\infty})^{-1}dU^{\infty} - F_3 T_3. \quad (16)$$

Using this calculation method, we verify that F_a are invariant for $J = [3/2, 2, 5/2, 3]$ under usual $SU(2)$ generator's representation [30].

C. Sphaleron under a $SU(2)$ scalar multiplet extension

In this subsection, we investigate the sphaleron configuration with a general high-dimensional $SU(2)$ scalar extension to the SM. This configuration was previously constructed by Ahriche et. al [29]. However, we present a different perspective on the unitary transformation matrix.

Consider N scalar multiplet fields, denoted as Φ^i with $i = 1, \dots, N$. In [29], the vacuum configurations of Φ^i are parameterized as

$$\Phi^i = \frac{v_i h_i(\xi)}{\sqrt{2}} (0, \dots, 1, \dots, 0)^T. \quad (17)$$

where v_i and h_i represent the scalar field's vev and radial profile function, respectively.

However, since there exists only a single $SU(2)$ sphaleron gauge transformation matrix, U^{∞} , it is in general not *a priori* clear that one choice can transform all scalar fields in phase II to the form in eq. (7) that carries no dependence on (μ, θ, ϕ) . To address this question, one should take into account the number of gauge transformation degrees of freedom. For concreteness, we consider the two Higgs doublet model (2HDM). In the 2HDM, we can perform an $SU(2)_L \times U(1)_Y$ transformation to a basis where the vev of neutral component of Φ^1 is real while the corresponding neutral component of Φ^2 is complex [31]

$$\Phi^1 = \begin{pmatrix} 0 \\ v_1 \end{pmatrix}, \quad \Phi^2 = \begin{pmatrix} 0 \\ v_2 e^{i\xi} \end{pmatrix}, \quad (18)$$

where v_1 and v_2 are real and positive, and $0 \leq \xi < 2\pi$. If we follow MK's sphaleron configuration, the field configurations for the 2HDM should be written as

$$\begin{aligned} \Phi^1 &= \frac{v_1}{\sqrt{2}} h_1(\xi) U^{\infty}(\mu, \theta, \phi) \begin{pmatrix} 0 \\ 1 \end{pmatrix}, \\ \Phi^2 &= \frac{v_2}{\sqrt{2}} h_2(\xi) U^{\infty}(\mu, \theta, \phi) \begin{pmatrix} 0 \\ e^{i\xi} \end{pmatrix} \\ &= \frac{v_2}{\sqrt{2}} h_2(\xi) U^{\infty}(\mu', \theta', \phi') \begin{pmatrix} 0 \\ 1 \end{pmatrix}, \end{aligned} \quad (19)$$

where $h_1(\xi)$ and $h_2(\xi)$ denote the radial profile function of two doublets, respectively. Generally, $\mu \neq \mu', \theta \neq \theta', \phi \neq \phi'$. In other words, the presence of a complex phase in the vacuum configuration that cannot be removed by a gauge transformation implies that there does not exist a single U matrix that can rotate both scalar fields to the form in eq. (7) for a common set of NCL parameters. Only for certain choices of the scalar potential parameters, for which $\xi = 0$, can one achieve such a common set. This situation should hold for a general dimensional electroweak multiplet extension of the SM, whose field configuration should be written as

$$\Phi = \frac{v_{\phi}}{\sqrt{2}} \phi(\xi) U^{\infty}(\mu', \theta', \phi') \begin{pmatrix} 0 \\ \dots \\ 1 \\ \dots \\ 0 \end{pmatrix}. \quad (20)$$

we seek for situations where $\mu = \mu', \theta = \theta', \phi = \phi'$. This requires additional constraints to the model parameters. As in the 2HDM, additional constraints should be applied to make $\xi = 0$. In section III, we will analyze these constraints carefully.

Assuming these constraints are satisfied, the sphaleron configuration proposed by Ahriche et al. can be directly applied. We provide a summary of their results for the sake of completeness. In the first and third phases, when $\mu \in [-\frac{\pi}{2}, 0]$ and $\mu \in [\pi, \frac{3\pi}{2}]$, the electroweak multiplet's configuration is

$$\Phi = \frac{v_{\phi}(\sin^2 \mu + \phi(\xi) \cos^2 \mu)}{\sqrt{2}} (0, \dots, 1, \dots, 0)^T, \quad (21)$$

In the second phase when $\mu \in [0, \pi]$, the field configuration is

$$\Phi = \frac{v_{\phi} \phi(\xi)}{\sqrt{2}} (0, \dots, 1, \dots, 0)^T. \quad (22)$$

D. The validity check of baryon charge

In general, one should ask how the presence of these additional multiplets affect the Cherns-Simons number and, thus, $B + L$, associated with the sphaleron configuration. In the case of $n = 2$ it has been shown that the sphaleron baryonic charge $Q_B = 1/2$, and the leptonic

charge of sphaleron is the same as the baryonic charge, leading to $Q_{B+L} = 1$ [23].

We now review the computation of Q_B , which can be written as [23]

$$Q_B(\text{sphaleron}) = \int_{-\infty}^{t_0} dt \int d^3x \left(\frac{g^2}{32\pi^2} F_{\mu\nu}^a \tilde{F}^{a\mu\nu} \right), \quad (23)$$

where t_0 represents the sphaleron configuration while $t = -\infty$ represents the vacuum. The dual field tensor $\tilde{F}^{a\mu\nu} = \frac{1}{2}\epsilon^{\mu\nu\rho\sigma} F_{\rho\sigma}^a$. Clearly, since eq. (12) leaves the 1-form F_a unchanged from the KL form, we will demonstrate that the value of Q_B will also be unchanged. To proceed with the latter, note that since $F_{\mu\nu}^a \tilde{F}^{a\mu\nu}$ can be written as a total divergence $\partial_\mu K^\mu$, with

$$K^\mu = \epsilon^{\mu\nu\rho\sigma} (F_{\nu\rho}^a A_\sigma^a - \frac{g}{3} f^{abc} A_\nu^a A_\rho^b A_\sigma^c), \quad (24)$$

so that

$$Q_B(\text{sphaleron}) = \frac{g^2}{32\pi^2} \left(\int d^3x K^0 \Big|_{t=t_0} + \int_{-\infty}^{t_0} dt \int_S \vec{K} \cdot d\vec{S} \right), \quad (25)$$

where $K^0 = 0$ at vacuum when $t = -\infty$, since the gauge field $A_i^a = 0$ at the vacuum configuration eq. (6). If we work out the explicit gauge field component A_i^a in eq. (7), we would see that $A_i^a \sim 1/r$, which means that the surface term in eq. (25) does not vanish. The sphaleron baryon charge is gauge invariant from the definition eq. (23), so that we can make a gauge transformation U_{charge} such that the gauge field A_i^a falls off faster than $1/r$. Such transformation can take the following form [32]

$$U_{\text{charge}} = \exp(-i\Omega(r)\hat{r} \cdot \vec{\sigma}), \quad \Omega(r) = \mu \tanh(\beta r), \quad (26)$$

where μ is the NCL parameter in the sphaleron configuration, β is a large number. Under such gauge transformation, the surface term would vanish [33]. The sphaleron baryon charge becomes

$$Q_B(\text{sphaleron}) = \int d^3x K^0 \Big|_{t=t_0} + \frac{2\mu - \sin(2\mu)}{2\pi} = \frac{1}{2}. \quad (27)$$

where the first term vanishes due to the gauge field goes faster than $1/r$ at spatial infinity, and the NCL parameter $\mu = \frac{\pi}{2}$ at the sphaleron point. The result eq. (27) implies that the sphaleron baryon charge is irrelevant to the detailed shape of the radial profile function $f(\xi)$ defined in eq. (7). As we will see below, within the electroweak multiplet extension of the SM, the multiplet field would bias the gauge field radial profile function to some extent, while keeping $Q_B(\text{sphaleron}) = 1/2$.

E. Sphaleron Energy and equation of motion

In the following computations, we utilize the KL configuration defined in eq. (6) and eq. (7). For the additional scalar multiplet, its configuration is established in eq. (21) and eq. (22).

It is convenient to define the sphaleron energy relative to that of the vacuum state in the configuration space, *viz*

$$E_{\text{sph}} = E(\mu = \frac{\pi}{2}) - E(\mu = -\frac{\pi}{2}), \quad (28)$$

where $E(\mu = \frac{\pi}{2})$ represents the sphaleron energy at the configuration space saddle point, while $E(\mu = -\frac{\pi}{2})$ depicts the vacuum state value. The general potential $V(H, \Phi)$ of Higgs field and multiplet Φ includes the Higgs potential, Higgs and Φ portal interaction and Φ self interaction terms. However, one need to pay attention that different choices can be made to give the potential value V at the origin, and different choices correspond to different sphaleron vacuum energies. However, since the relevant quantity is the energy difference eq. (28), these different choices will have no physical consequence.

For example, we can write the Higgs field potential into two forms, one is $-\mu^2 H^\dagger H + \lambda(H^\dagger H)^2$, another is $\lambda(H^\dagger H - \frac{1}{2}v^2)^2$. In the former case, we should carefully consider the sphaleron vacuum state value and the situation would be more complicated if more scalar fields enter the potential.

In the following analysis, we construct the sphaleron energy using one scalar multiplet's extension to the SM. Meanwhile, it is sufficient to use $V(H, \Phi)$ as a general object to demonstrate the main ideas in this section. We will present the explicit interaction terms in the next section. With one multiplet's extension to the SM, either term in the right hand side of eq. (28) can be written as

$$E = \frac{4\pi\Omega}{g} \int d\xi \left[\frac{1}{4} F_{ij}^a F_{ij}^a + \frac{1}{4} f_{ij}^a f_{ij}^a + (D_i H)^\dagger (D_i H) + (D_i \Phi)^\dagger (D_i \Phi) + V(H, \Phi) \right], \quad (29)$$

when $\mu = -\frac{\pi}{2}$, the Yang-Mills term, U(1) term, and kinetic term both equal to trivial zero, since the gauge fields are empty and the scalar fields are in vacuum states; while when $\mu = \frac{\pi}{2}$, these three terms' formal computation are carried out in Appendix B. Therefore, the only undetermined terms in eq. (28) are $V(H, \Phi)(\xi, \mu = \frac{\pi}{2})$ and $V(H, \Phi)(\xi, \mu = -\frac{\pi}{2})$. Thus, the sphaleron energy can be expressed as

$$\begin{aligned}
E_{\text{sph}} &= E(\mu = \frac{\pi}{2}) - E(\mu = -\frac{\pi}{2}) \\
&= \frac{4\pi\Omega}{g} \int d\xi \left[\frac{1}{4} F_{ij}^a F_{ij}^a(\xi, \mu = \frac{\pi}{2}) + \frac{1}{4} f_{ij} f_{ij}(\xi, \mu = \frac{\pi}{2}) + (D_i H)^\dagger (D_i H)(\xi, \mu = \frac{\pi}{2}) + (D_i \Phi)^\dagger (D_i \Phi)(\xi, \mu = \frac{\pi}{2}) \right. \\
&\quad \left. + V(H, \Phi)(\xi, \mu = \frac{\pi}{2}) - V(H, \Phi)(\xi, \mu = -\frac{\pi}{2}) \right].
\end{aligned} \tag{30}$$

The field's equation of motion (EOM) can be obtained via the Euler-Lagrangian equation. In our analysis, there

are two scalar fields, H and Φ . Similar to the case in Ahriche et al.'s work [29], the EOMs reads

$$\begin{aligned}
f'' + \frac{2}{\xi^2} (1-f) [f(f-2) + f_3(1+f_3)] + (1-f) \left(\frac{v^2 h^2}{4\Omega^2} + \alpha \phi^2 \right) &= 0, \\
f_3'' - \frac{2}{\xi^2} [3f_3 + f(f-2)(1+2f_3)] + \left(\frac{v^2}{4\Omega^2} h^2 + \beta \phi^2 \right) (f_0 - f_3) &= 0, \\
f_0'' + \frac{2}{\xi^2} (1-f_0) - \frac{g'^2}{g^2} \left(\frac{v^2}{4\Omega^2} h^2 + \beta \phi^2 \right) (f_0 - f_3) &= 0, \\
h'' + \frac{2}{\xi} h' - \frac{2}{3\xi^2} h [2(1-f)^2 + (f_0 - f_3)^2] - \frac{1}{g^2 v^2 \Omega^2} \frac{\partial V[h, \phi]}{\partial h} &= 0, \\
\phi'' + \frac{2}{\xi} \phi' - \frac{8\Omega^2 \phi}{3v^2 \xi^2} [2\alpha(1-f)^2 + \beta(f_0 - f_3)^2] - \frac{1}{g^2 v^2 \Omega^2} \frac{\partial V[h, \phi]}{\partial \phi} &= 0,
\end{aligned} \tag{31}$$

where f' denotes $df/d\xi$ and f'' denotes $d^2f/d\xi^2$. In the zero temperature computation, we set $v = \Omega = 246.22$ GeV. However, at high temperature universe, v is a function of the temperature; Ω is just a dimensional constant; and α and β are defined as

$$\alpha = \frac{[J(J+1) - J_3^2] v_\phi^2}{2\Omega^2}, \quad \beta = \frac{J_3^2 v_\phi^2}{\Omega^2}. \tag{32}$$

where J denotes the multiplet representation dimension, and J_3 is the third component value. Since we put the multiplet's vev in its neutral component, J_3 equals to the opposite value of hypercharge Y . The only undefined term in EOMs (31) is the potential term $V[h, \phi]$, which is related with BSM models and types of EWPT.

F. Boundary conditions of the sphaleron EOM

In this subsection, we will clarify some subtleties regarding the sphaleron EOM boundary conditions. The boundary condition for scalar fields at spatial infinity is clear: each field should approach its vacuum. On the other hand, at the origin, some subtleties would appear, depending on the choice of co-ordinate system. At this location, the scalar field profile function boundary condition shares common features with gauge field

ones. Therefore, we can mainly focus on gauge field profile function boundary condition analysis. Working with spherical-polar co-ordinates, the usual criteria for boundary condition can be summarized as [22, 23]

- when $\xi \rightarrow 0$, the field is free of singularity,
- when $\xi \rightarrow \infty$, the gauge field should vanish to ensure the finiteness of sphaleron energy, where $A_i^a = 0$ is equivalent to the pure gauge state $A_i^a dx^i \sim \partial_i (U^\infty)^{-1} U^\infty$ up to a gauge transformation.

In this work, we have different opinions to above two criteria and propose following additional condition

- when $\xi \rightarrow \infty$, if we set the boundary condition as $f(\xi \rightarrow \infty) = C$, the field profile function should converge to the chosen constant value C . In such case, either the scalar field or the gauge field can converge to the vacuum state, where we do not expect the profile function to have any rapid changes around vacuum configuration.

Let us elaborate on the singularity issue. According to MK configuration eq. (4), U^∞ is a function of angular parameters θ, ϕ . When $r \rightarrow 0$, if the field does not vanish, the field would have some preferred angular direction at the origin, which can lead to a rotational singularity. In

the following, we will demonstrate that such singularity is removable.

As we show in section II A, a unitary gauge transformation can connect following two field configurations under the zero weak mixing angle scenario

$$-f(\xi) \sum_a F_a J_a \xrightarrow{U^\infty} [1 - f(\xi)] \sum_a F_a J_a, \quad (33)$$

which means such a gauge transformation can interchange the boundary condition at the origin and spatial infinity. For example, following two sets of boundary conditions can be converted to each other by such a gauge transformation.

- (a) $\xi \rightarrow 0, f(\xi) \rightarrow 0; \xi \rightarrow \infty, f(\xi) \rightarrow 1;$
- (b) $\xi \rightarrow 0, f(\xi) \rightarrow 1; \xi \rightarrow \infty, f(\xi) \rightarrow 0.$

Thus, when $\xi \rightarrow 0$, the free of singularity condition is not strict. Since we can always make such gauge transformation to remove the singularity. In fact, the two criteria at the beginning of this subsection can be turned into

- sphaleron has finite energy

A finite sphaleron energy requires that (i) the field is free of singularities everywhere, and (ii) the integrand of eq. (30) vanishes when $\xi \rightarrow \infty$. For (ii), when $\xi \rightarrow \infty$, the gauge field and scalar field approaching the vacuum condition can make the Yang-Mills, U(1), and kinetic terms vanish, and equate the terms $V(H, \Phi)(\xi, \mu = \frac{\pi}{2})$ and $V(H, \Phi)(\xi, \mu = -\frac{\pi}{2})$. As we have shown, both gauge field boundary conditions (a) and (b) can lead to a finite sphaleron energy. Under such a situation, we should consider the third convergence condition that has been proposed in this work, which can be used to distinguish between (a) and (b).

Now, for our specific sphaleron configuration eq. (7), If we only consider the first two criteria, we can have two sets of boundary condition, where we label them as Normal boundary condition and Inverse boundary condition. For the Normal condition, we have

$$\begin{aligned} \text{for } \xi \rightarrow 0, \{f(\xi), f_3(\xi), h(\xi), \phi(\xi)\} &\rightarrow 0, f_0(\xi) \rightarrow 1; \\ \text{for } \xi \rightarrow \infty, \{f(\xi), f_3(\xi), h(\xi), \phi(\xi), f_0(\xi)\} &\rightarrow 1; \end{aligned} \quad (34)$$

While the Inverse Boundary condition reads

$$\begin{aligned} \text{for } \xi \rightarrow 0, \{f(\xi), f_3(\xi)\} &\rightarrow 1, \{f_0(\xi), h(\xi), \phi(\xi)\} \rightarrow 1; \\ \text{for } \xi \rightarrow \infty, \{f(\xi), f_3(\xi)\} &\rightarrow 0, \{f_0(\xi), h(\xi), \phi(\xi)\} \rightarrow 1. \end{aligned} \quad (35)$$

The field profile functions and sphaleron energy of the SM under these two boundary choices are shown in Figure 2. These two scenarios' sphaleron energy are very similar, where the Inverse boundary choice is a little bit larger than the Normal one. However, the third convergence condition requires us to choose the Normal Boundary condition, since the field profile functions vary rapidly when $\xi \rightarrow \infty$ for the Inverse boundary scenario.

III. ELECTROWEAK SEPTUPLET EXTENSION TO THE SM: MODEL ANALYSIS

In this section, we will analyze the scalar septuplet extension to the SM under different EWPT scenarios, using the formalism outlined in Section II. As a prelude, let us review the motivation for focusing on the scalar septuplet. In general, for an electroweak multiplet having isospin J , J cannot be arbitrarily large. When $J \geq 5$, the Landau scale at which the gauge coupling Landau pole occurs would decrease to around $\Lambda_{\text{landau}} \leq 10$ TeV [34]. Furthermore, the partial wave unitarity condition for tree-level scattering amplitude constrains $J \leq 7/2$ for a complex scalar multiplet and $J \leq 4$ for a real scalar multiplet [35, 36]. Besides, we are more focused on the neutral component of the multiplet, where the charge relation $J_3 + Y = 0$ needs to be satisfied. Furthermore, in order to avoid stringent dark matter experimental direct detection constraints we require that the neutral field does not couple to Z current, which requires $Y = 0$. Since only multiplet with integer J can have $J_3 = 0$ component, we will focus on this scenario. Such electroweak multiplet with zero vev can be a dark matter candidate [37, 38]. Thus, the highest dimension for an electroweak multiplet satisfying the unitary condition and providing a viable dark matter candidate is the septuplet with $J = 3$ [38]. Therefore, the sphaleron energy computation with a septuplet extension to the SM is carried out in this study.

As discussed in the introduction, we consider three patterns of EWSB, as shown in Figure 1. Figure 1 (a) shows the one-step EWPT to pure Higgs phase, where the additional scalar can change the Higgs phases' sphaleron energy through thermal loops. In principle, the thermal loop corrections should also be included when analyzing patterns (b) or (c), since the EWSB occurs at hot early universe. The three dimensional effective field theory (3dEFT) is a powerful analytic method to organize the thermal corrections [39–41]. There are recent applications of 3dEFT to the nucleation rate computation [42, 43], whose results show that the thermal correction would bias the zero temperature four dimensional model parameters (including vev) to some extent. However, zero temperature analysis can still provide a useful baseline for subsequent $T > 0$ analyses. In our present work, we mainly aim to provide a methodology for applying the sphaleron formalism into different EWSB patterns, so the zero temperature analysis is a good and clear start point. When the temperature effect is included, the analysis strategy can be applied to the thermal potential. For our current zero-temperature analysis, we are more interested in case (b) and (c). We label the vevs of the scalar potential stationary points in Figure 1 as, $X(v_x, 0)$, $Y(0, v_y)$ and $Z(v_{zx}, v_{zy})$. In general, $v_{zx} \neq v_x$ and $v_{zy} \neq v_y$. Further more, when we parameterize the scalar fields and perform a model analysis, we usually regard the field vevs as input parameter. Thus, for patterns (b) and (c), we cannot use one single model analysis

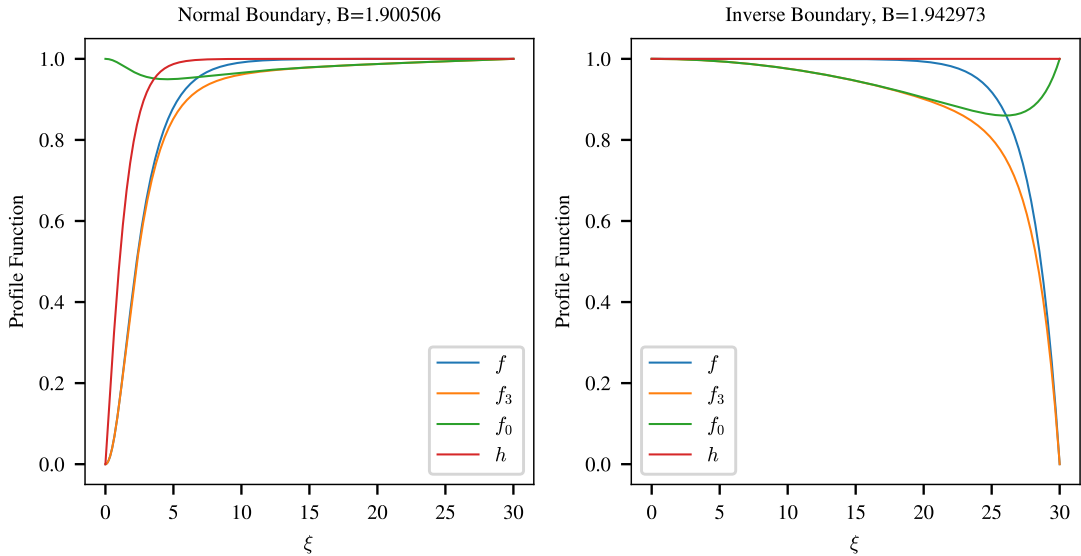


Figure 2: Two sets of profile functions in the standard model. Left figure denotes the field solutions under Normal boundary condition that has been used in previous works, see Refs. [22, 24, 29]. Right figure represents the solutions under the Inverse boundary condition. The horizontal axis is a dimensionless radial parameter $\xi = g\Omega r$, where $\Omega = 246$ GeV and g is the SU(2) gauge coupling constant. In each figure's caption, we label the sphaleron energy B value, where the formal expression $E_{\text{sph}} = B \cdot (4\pi\Omega)/g$ is defined in eq. (61). We can observe that, apart from the Higgs field profile function, the solutions of other gauge fields behave like the vertical mirror of the ones in the left figure.

strategy, since the required input vevs and model parameter relationships may differ in different EWSB patterns. We will show two analysis strategies separately after the introduction of the model.

A. The Model

The general potential of the SM Higgs H and another SU(2) multiplet Φ can be written as [37]

$$\begin{aligned}
 V = & M_A^2 (\Phi^\dagger \Phi) + \{ M_B^2 (\Phi\Phi)_0 + \text{h.c.} \} \\
 & - \mu^2 H^\dagger H + \lambda (H^\dagger H)^2 + \lambda_1 (H^\dagger H) (\Phi^\dagger \Phi) \\
 & + \lambda_2 ((\bar{H}H)_1 (\bar{\Phi}\Phi)_1)_0 + [\lambda_3 (\bar{H}H)_0 (\Phi\Phi)_0 + \text{h.c.}] \\
 & + V_{\text{self}}(\Phi, \bar{\Phi}),
 \end{aligned} \tag{36}$$

with

$$\begin{aligned}
 V_{\text{self}}(\Phi, \bar{\Phi}) = & \sum_{J=0}^{2J} \kappa_k ((\Phi\Phi)_k (\bar{\Phi}\bar{\Phi})_k)_0 \\
 & + \sum_{k=0}^{2J} \{ \kappa'_k ((\Phi\Phi)_k (\Phi\Phi)_k)_0 \\
 & + \kappa''_k ((\bar{\Phi}\bar{\Phi})_k (\Phi\Phi)_k)_0 + \text{h.c.} \}.
 \end{aligned} \tag{37}$$

where J is the multiplet isospin index, and $J = 3$ is the septuplet case. The scalar multiplet self-interaction potential $V_{\text{self}}(\Phi, \bar{\Phi})$ may be important in solving the core-cusp problem [44, 45]. The \bar{H} and $\bar{\Phi}$ are the complex conjugate representation of H and Φ . As pointed out

in [37], the terms $(\Phi\Phi)_1$, $(\Phi\Phi)_3$ and $(\Phi\Phi)_5$ vanish due to the property of Clebsch-Gordan coefficients. Therefore, for the self interaction potential, only terms with $k \in [0, 2, 4, 6]$ have non-zero contributions. Further more, only terms with $k = 0, 2$ are independent for our septuplet example [37, 46], which simplifies our model analysis.

B. One-step EWPT to the mixed phase

In this pattern, we parameterize the general complex Higgs field (H), septuplet field (Φ) and their complex conjugate representation (\bar{H} , $\bar{\Phi}$) as

$$H = \begin{pmatrix} \omega^+ \\ \frac{1}{\sqrt{2}}(v+h+i\pi) \end{pmatrix}; \bar{H} = \begin{pmatrix} \frac{1}{\sqrt{2}}(v+h-i\pi) \\ -\omega^- \end{pmatrix}, \tag{38}$$

$$\Phi = \begin{pmatrix} \phi_{3,3} \\ \phi_{3,2} \\ \phi_{3,1} \\ \frac{1}{\sqrt{2}}(v_\phi + \phi + i\pi_\phi) \\ \phi_{3,-1} \\ \phi_{3,-2} \\ \phi_{3,-3} \end{pmatrix}; \bar{\Phi} = \begin{pmatrix} \phi_{3,-3}^* \\ -\phi_{3,-2}^* \\ \phi_{3,-1}^* \\ -\frac{1}{\sqrt{2}}(v_\phi + \phi - i\pi_\phi) \\ \phi_{3,1}^* \\ -\phi_{3,2}^* \\ \phi_{3,3}^* \end{pmatrix}. \tag{39}$$

where v and v_ϕ are vevs of the Higgs field and septuplet field, respectively. We put the septuplets vev into its neutral component, where the neutral fields are unconstrained by the Z current experiment. As discussed in Section II C, additional constraints need to be applied

if we put the Higgs and septuplet's vevs both into real neutral components. This can be fulfilled by requiring all the fluctuation fields (inside Higgs or septuplet) have positive mass eigenvalues. Before that, one important constraint is from the tadpole condition

$$\left. \frac{\partial V}{\partial x_i} \right|_{\forall x_i=0} = 0, \quad (40)$$

where $x_i \in [h, \pi, \omega^\pm, \phi, \pi_\phi, \phi_{3,j}, \phi_{3,j}^*]$; j denotes the various subscripts that appear in Φ ; and $\forall x_i = 0$ means set all the field fluctuations equal to zero after the partial derivative. Subsequently, we can obtain five parameter constraints

$$\begin{aligned} \text{Im}(M_B^2) &= \text{Im}(\lambda_3) = 0, \\ \text{Im}(\kappa_0'') - 2\text{Im}(\kappa_0') + \frac{4(\text{Im}(\kappa_2'') - 2\text{Im}(\kappa_2'))}{3\sqrt{5}} &= 0, \\ \mu^2 &= \lambda v^2 + \lambda_{13} v_\phi^2, \\ M_A^2 - \frac{2}{\sqrt{7}} \text{Re}(M_B^2) &= -\lambda_s v_\phi^2 - \lambda_{13} v^2, \end{aligned} \quad (41)$$

where the first three constraints actually arise from one condition: $\partial V / \partial \pi = 0$. We convert this single tadpole constraint into three separate constraints, which can eliminate the mixing between h and π_ϕ and simplify our analysis. In addition, λ_{13} and λ_s are two combined parameters

$$\lambda_{13} = \frac{1}{2} \lambda_1 - \frac{1}{\sqrt{14}} \lambda_3, \quad (42)$$

$$\begin{aligned} \lambda_s &= + \frac{1}{7} [\kappa_0 + 2\text{Re}(\kappa_0') - 2\text{Re}(\kappa_0'')] \\ &+ \frac{4}{21\sqrt{5}} [\kappa_2 + 2\text{Re}(\kappa_2') - 2\text{Re}(\kappa_2'')]. \end{aligned} \quad (43)$$

As discussed in Ref. [37], λ_{13} enters the DM annihilation and direct detection rates, while λ_s characterizes DM self-interactions.

The total potential can be expressed as a series addition of mass matrices:

$$\begin{aligned} V(H, \Phi) &= \frac{1}{2} \begin{pmatrix} h & \phi \end{pmatrix} \mathbf{H}_{2 \times 2} \begin{pmatrix} h \\ \phi \end{pmatrix} + \frac{1}{2} \begin{pmatrix} \pi & \pi_\phi \end{pmatrix} \mathbf{P}_{2 \times 2} \begin{pmatrix} \pi \\ \pi_\phi \end{pmatrix} \\ &+ \begin{pmatrix} \omega^+ & \phi_{3,1} & \phi_{3,-1}^* \end{pmatrix} \mathbf{C}_{1 \times 3} \begin{pmatrix} \omega^- \\ \phi_{3,1}^* \\ \phi_{3,-1} \end{pmatrix} \\ &+ \begin{pmatrix} \phi_{3,2} & \phi_{3,-2}^* \end{pmatrix} \mathbf{C}_{2 \times 2} \begin{pmatrix} \phi_{3,2}^* \\ \phi_{3,-2} \end{pmatrix} \\ &+ \begin{pmatrix} \phi_{3,3} & \phi_{3,-3}^* \end{pmatrix} \mathbf{C}_{3 \times 2} \begin{pmatrix} \phi_{3,3}^* \\ \phi_{3,-3} \end{pmatrix}. \end{aligned} \quad (44)$$

where we put the explicit mass matrix expression in Appendix C. As expected, we observe a massless pseudo-scalar particle and a massless charged Higgs particle after the computation of matrix eigenvalues. The matrix

$\mathbf{P}_{2 \times 2}$ has one non-zero eigenvalue and $\mathbf{C}_{1 \times 3}$ has two non-zero eigenvalues.

Let us now enumerate the constraints that we need to apply. If this number plus the quantity of input parameters is less than or equal to the total parameters' degrees of freedom, we are free to move on. On the one hand, a non-negative mass matrix eigenvalues require 9 constraints: 1 from $\mathbf{P}_{2 \times 2}$, 2 from each other four matrices. Also, we have 5 tadpole constraints, so we have 14 parameter constraints. On the other hand, we have 19 degrees of freedom from the the model eq. (36) (note that some parameters are complex and we need to count the SM two parameters). So in total we can set 5 independent input parameters for this model. We take these 5 input parameters to be $v, v_\phi, \lambda, \lambda_{13}$ and λ_s , and they will appear in our later potential analysis. After these constraints, we are able to set $\mu = \mu', \theta = \theta', \phi = \phi'$ in eq. (20).

Now, we can compute the sphaleron energy. According to sphaleron Higgs and multiplet configuration eq. (7) and eq. (22), we need to set all the fluctuation fields in eq. (38) and eq. (39) equal to zero. Then, make the following replacement

$$v \rightarrow h[\xi]v, \quad v_\phi \rightarrow \phi[\xi]v_\phi, \quad (45)$$

we can obtain the final potential formula in one-step EWPT as

$$\begin{aligned} V_{\text{One}}(\xi, \mu = \frac{\pi}{2}) &= \frac{1}{2} v_\phi^2 \phi[\xi]^2 [\lambda_{13} v^2 h(\xi)^2 - (v_\phi^2 \lambda_s + \lambda_{13} v^2)] \\ &+ \frac{1}{4} v^2 h[\xi]^2 [\lambda v^2 h(\xi)^2 - 2(\lambda v^2 + \lambda_{13} v_\phi^2)] \\ &+ \frac{1}{4} v_\phi^4 \lambda_s \phi[\xi]^4, \end{aligned} \quad (46)$$

where V_{One} represents the one-step EWPT to the mixed phase. The vacuum potential reads

$$V_{\text{One}}(\xi, \mu = -\frac{\pi}{2}) = -\frac{1}{4} (v_\phi^4 \lambda_s + \lambda v^4 + 2\lambda_{13} v_\phi^2 v^2). \quad (47)$$

Thus far, we have finished the last task needed to solve the EOM and compute the sphaleron energy. Equations (46) and (47) multiplied by the normalization factor $\frac{\xi^2}{g^2 \Omega^4}$ constitute the potential that appear in eq. (30). However, for the potential term $V[h(\xi), \phi(\xi)]$ that appear in EOMs (31), we should directly use eq. (46) without any such normalization factors.

C. Two-step EWPT

For this EWPT pattern, as demonstrated previously, the analysis method should be different from one-step case, since the v and v_ϕ in as computed for the one-step scenario do not correspond to the true vevs now. However, we will continue to use v and v_ϕ to denote the Higgs and septuplet vev in this subsection, keeping in

mind that they do not bear any relationship with one-step values.

First, we expand the Higgs and septuplet fields around their extremal scalar field configuration

$$H = \frac{h}{\sqrt{2}} \begin{pmatrix} 0 \\ 1 \end{pmatrix}, \quad \Phi = \frac{\phi}{\sqrt{2}} \begin{pmatrix} 0 \\ 0 \\ 0 \\ 1 \\ 0 \\ 0 \\ 0 \end{pmatrix}, \quad (48)$$

Then, substitute eq. (48) into eq. (36), we can obtain a general potential expression V_{general} . Secondly, apply the tadpole criteria

$$\frac{\partial V_{\text{general}}}{\partial h} = \frac{\partial V_{\text{general}}}{\partial \phi} = 0, \quad (49)$$

we can obtain nine extremal points, which have a \mathbb{Z}_2 symmetry. These nine extremal points can be shown by mirroring Figure 1 (c) to all four quadrants. Figure 1 (c)'s X, Y and Z point's vev and their hessian determinant are summarized in Table I, where we have defined a new set of parameters

$$\begin{aligned} v &= \frac{\mu}{\sqrt{\lambda}}, \quad v_\phi = \frac{\sqrt{2\sqrt{7}M_B^2 - 7M_A^2}}{\sqrt{7\lambda_s}}, \\ v_z^2 &= \frac{\lambda_s (\lambda_{13}v_\phi^2 - \lambda v^2)}{\lambda_{13}^2 - \lambda\lambda_s}, \\ v_{z\phi}^2 &= \frac{\lambda(\lambda_{13}v^2 - v_\phi^2\lambda_s)}{\lambda_{13}^2 - \lambda\lambda_s}, \\ V_z &= v_\phi^4\lambda_s + \lambda v^4 - 2\lambda_{13}v_\phi^2v^2, \end{aligned} \quad (50)$$

where the definition of λ_{13} is same with eq. (42). We notice that the relationship between vevs and model parameters are different from one-step EWPT to mixed phase eq. (41). In the one-step EWPT, v and v_ϕ should be interpreted as v_z and $v_{z\phi}$ shown in Table I. One can verify that, inside eq. (50), if we put the expression of v and v_ϕ into v_z^2 and $v_{z\phi}^2$, the v_z^2 and $v_{z\phi}^2$ have following relation

$$\begin{aligned} \mu^2 &= \lambda v_z^2 + \lambda_{13}v_{z\phi}^2, \\ M_A^2 - \frac{2\text{Re}(M_B^2)}{\sqrt{7}} &= -\lambda_{13}v_z^2 - \lambda_s v_{z\phi}^2. \end{aligned} \quad (51)$$

This is just the last two relations in eq. (41), so the two analysis methods are consistent with each other. Let us elaborate further on the mass matrix in the two-step EWPT. The calculational methods should be quite parallel with one-step scenario, where we need to start from the general field parameterization eq. (38) and eq. (39). While, the difference comes from the relationship between vevs and model parameters. Therefore, we can obtain the various mass matrices in eq. (44), but with different parameter relationships.

Returning to our potential analysis, we can express the potential as

$$V_{\text{general}} = \frac{1}{4}[\phi^2(2h^2\lambda_{13} - 2v_\phi^2\lambda_s) + h^2(h^2\lambda - 2\lambda v^2) + \phi^4\lambda_s]. \quad (52)$$

For purposes of deriving and solving the EOM and computing the sphaleron energy, we need to make the substitution $h \rightarrow h[\xi]v, \phi \rightarrow \phi[\xi]v_\phi$. Then the potential reads

$$\begin{aligned} V_{\text{Two}}(\xi, \mu = \frac{\pi}{2}) &= \frac{1}{4}h[\xi]^2v^2(h[\xi]^2v^2\lambda - 2\lambda v^2) + \frac{1}{4}\phi[\xi]^4v_\phi^4\lambda_s \\ &+ \frac{1}{2}\phi[\xi]^2v_\phi^2(h[\xi]^2v^2\lambda_{13} - v_\phi^2\lambda_s). \end{aligned} \quad (53)$$

where V_{Two} represent potential in two-step EWPT scenario, which has the identical property with eq. (46) in the sphaleron energy computation.

The vacuum potential in two-step EWPT reads

$$V_{\text{Two}}(\xi, \mu = -\frac{\pi}{2}) = -\frac{1}{4}(v_\phi^4\lambda_s + \lambda v^4 - 2\lambda_{13}v_\phi^2v^2). \quad (54)$$

To fulfill a two-step EWPT, additional parameter constraints should be applied. As shown in Figure 1 (c), we require our universe undergoes from $O \rightarrow Y \rightarrow X$. Here are the requirements

1. O must be a secondary local minimum, this require

$$\lambda_s > 0, \quad (55)$$

2. $V(Y) > V(X)$, this implies

$$\lambda_s v_\phi^4 < \lambda v^4, \quad (56)$$

3. $\text{Hess}(X) > 0$, this require

$$\lambda_{13}v^2 - v_\phi^2\lambda_s > 0, \quad (57)$$

4. $\text{Hess}(Y) > 0$, this implies

$$\lambda_{13}v_\phi^2 - \lambda v^2 > 0, \quad (58)$$

5. if we require the point M exist, we need to solve the equations:

$$\begin{aligned} v_z^2 &= \frac{\lambda_s (\lambda_{13}v_\phi^2 - \lambda v^2)}{\lambda_{13}^2 - \lambda\lambda_s}, \\ v_{z\phi}^2 &= \frac{\lambda(\lambda_{13}v^2 - v_\phi^2\lambda_s)}{\lambda_{13}^2 - \lambda\lambda_s}, \end{aligned} \quad (59)$$

with the constraints eq. (57) and eq. (58), the conditions $v_z^2 > 0$ and $v_{z\phi}^2 > 0$ require

$$\lambda_{13}^2 - \lambda\lambda_s > 0. \quad (60)$$

one would observe that $\text{Hess}(M) < 0$ under all above criteria, so the mixed point is not a stationary point.

Table I: Parameter table for the two-step EWPT.

	h	ϕ	V	Hessian Determinant
O	0	0	0	$\lambda\lambda_s v^2 v_\phi^2$
X	v	0	$-\frac{1}{4}\lambda v^4$	$2\lambda v^2 (\lambda_{13} v^2 - v_\phi^2 \lambda_s)$
Y	0	v_ϕ	$-\frac{1}{4}\lambda_s v_\phi^4$	$2v_\phi^2 \lambda_s (\lambda_{13} v_\phi^2 - \lambda v^2)$
Z	v_z	$v_{z\phi}$	$\frac{\lambda\lambda_s V_z}{4(\lambda_{13}^2 - \lambda\lambda_s)}$	$\frac{4\lambda\lambda_s (\lambda v^2 - \lambda_{13} v_\phi^2)(\lambda_{13} v^2 - v_\phi^2 \lambda_s)}{\lambda_{13}^2 - \lambda\lambda_s}$

These constraints are not totally independent, since the constraint eq. (57) can be derived out from eq. (56) and eq. (58), and the latter two conditions are of crucial importance. Overall, we again have five input parameters: $v, v_\phi, \lambda, \lambda_s$ and λ_{13} . The parameter ranges that satisfy the two-step EWPT are shown in Figure 3. In this plot, the lower bound is constrained by eq. (56), while the right vertical bound is constrained by eq. (58). The smaller the value of λ_s , the larger unconstrained parameter region we would have. At the end of the first step, constrained by the effective portal coupling, the septuplet vev cannot be arbitrarily small.

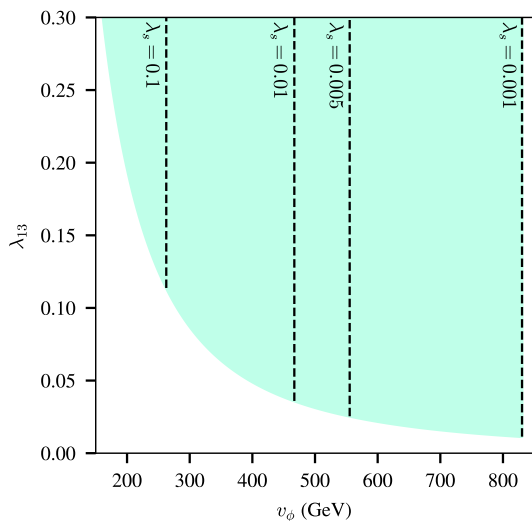


Figure 3: Parameter ranges that satisfy the two-step EWPT. The intersection of aquamarine color region and left hand side of λ_s vertical dashed line represents the feasible parameter region. The larger value of λ_s , the smaller viable parameter region.

IV. SPHALERON ENERGY WITH DIFFERENT EWPT SCENARIOS

The formal sphaleron energy can be defined as [47]

$$E_{\text{sph}} = B \cdot \frac{4\pi\Omega}{g} \quad (61)$$

where $\Omega = 246.22$ GeV and g is the weak coupling constant. The sphaleron B value is the integral part of

eq. (30). In the SM, where the EWPT is shown in pattern (a) in Figure 1, the sphaleron $B = 1.900506$. We will compute the sphaleron B value in pattern (b) and (c) in this subsection.

A. One-Step EWPT to the Mixed Phase

In this situation, both Higgs field and septuplet field obtain vev after the phase transition, while the v_ϕ should be constrained by the ρ parameter. The ρ parameter under multiple electroweak scalars is defined as

$$\rho = \sum_i \frac{[J_i(J_i + 1) - Y_i^2]v_i^2}{2Y_i^2 v_i^2}, \quad (62)$$

where J_i is the total isospin, Y_i denotes the hypercharge. In our situation, we have two scalar fields, one is the higgs field with $J = \frac{1}{2}$ and $Y = \frac{1}{2}$, another is the additional multiplet with J and $Y = 0$. Then, the ρ parameter is given by

$$\rho = 1 + 2J(J + 1) \frac{v_\phi^2}{v^2}, \quad (63)$$

the larger the multiplet representation, the stronger constraints are imposed on v_ϕ . According to the newest ρ parameter [48], $\rho = 1.00038 \pm 0.00020$. Within 95% significance level, v_ϕ is constrained to

$$v_\phi^2 \lesssim \frac{23.401}{J(J + 1)} \text{GeV} \quad (64)$$

so for our septuplet case, we are safe to take $v_\phi = 1$ GeV.

The computation of sphaleron energy can be separated into two parts: (i) obtain the field's profile solution from the EOMs (31); (ii) put the field's solution into the sphaleron energy expression eq. (30). For the first step, we present the field's profile function solution in Figure 4 (left figure) under the parameter choice $\lambda_{13} = 0.05$ and $\lambda_s = 0.005$. The field's profile solutions have a good convergence when $\xi \rightarrow \infty$. The sphaleron energy in this parameter choice is $B = 1.900535$, which is quite close to the SM B value. Apart from this, we perform a parameter scan to compute the sphaleron energy, which result is shown in Figure 5. Since the vev of v_ϕ is overwhelmingly small, the sphaleron energy differs little from pure SM case. Nevertheless, we observe that the multiplet effective self coupling λ_s almost doesn't influence the sphaleron energy. While, the larger value of effective portal coupling λ_{13} , the greater value of sphaleron energy. This relationship can be inferred from the one-step potential eq. (46) under a small value of v_ϕ . Therefore, in one-step EWPT scenario, if we only consider one scalar multiplet extension, the additional multiplet has negligible influence to the SM sphaleron energy constrained by the ρ parameter. We would like to make some comments about Georgi-Machacek model [18] where for more than one additional EW multiplet, the vevs for the new multiplets can be large, but the ρ parameter constraint is

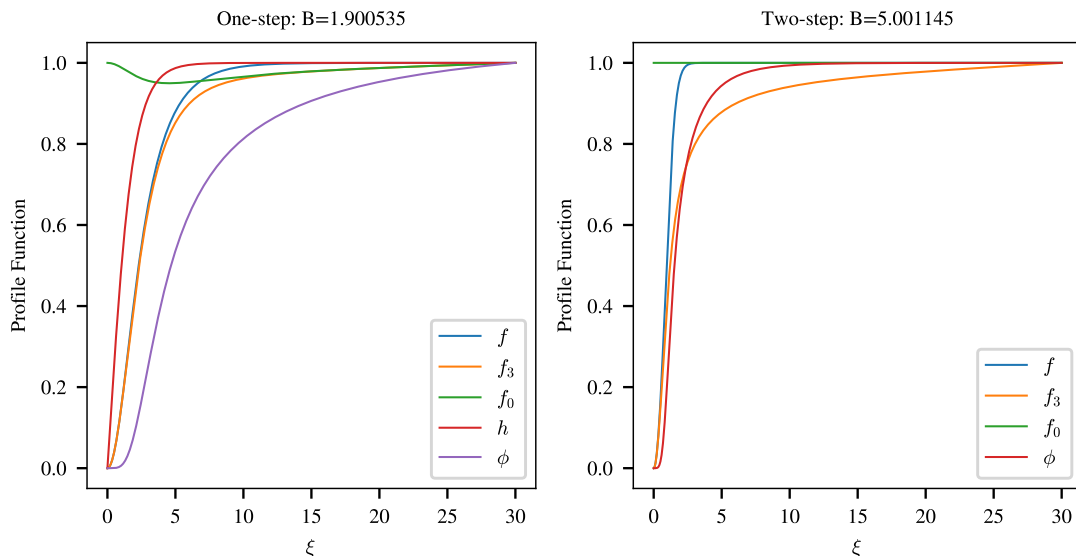


Figure 4: The radial profile functions in different EWPT patterns. Left figure denotes the EWPT to the mixed phase, where we take $v_\phi = 1$ GeV, $\lambda_{13} = 0.05$ and $\lambda_s = 0.005$. In this scenario, both the Higgs field h and multiplet field ϕ obtain vev, and the sphaleron energy value $B = 1.900535$. Right figure represents the two-step EWPT (at point Y of pattern (c) in Figure 1), where we take $v = 0$ GeV, $v_\phi = 500$ GeV, $\lambda_{13} = 0.05$ and $\lambda_s = 0.005$. At this stage, the Higgs field's profile function doesn't appear due to its vanishing vev, and sphaleron energy value in this stage is $B = 5.001145$.

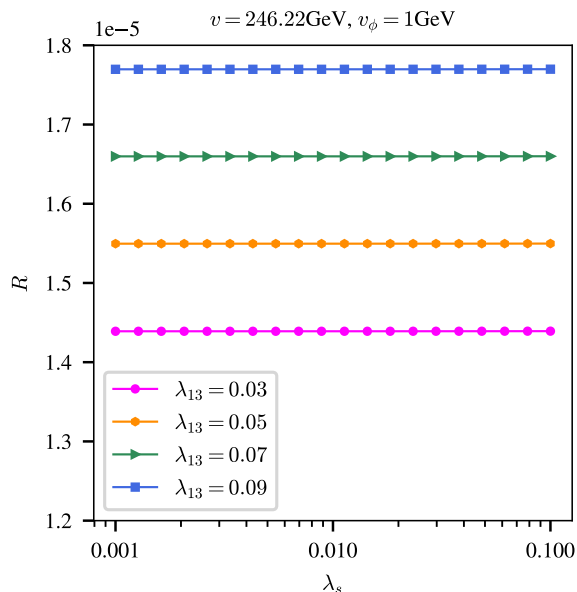


Figure 5: Sphaleron energy in one-step EWPT to mixed phase. The vertical axis $R = (E_{\text{Mixed}} - E_{\text{SM}})/E_{\text{SM}}$ is the sphaleron energy relative change with respect to the SM scenario. The SM sphaleron energy is $B = 1.900506$. Note that there is a 10^{-5} factor in the vertical axis. The Higgs vev is taken to be $v = 246.22$ GeV, and the multiplet's vev is chosen as $v_\phi = 1$ GeV.

satisfied. The formalism to analyze this case will be the same is discussed here, but then including one additional field vev. We might anticipate a significantly different result for the sphaleron energy in this case. We defer a

detailed study to future work.

B. Two-step EWPT

Since the modification of sphaleron energy in one-step case is very small, we are more interested for two-step EWPT scenario. As shown in Figure 1 (c), the first step is $C1 : O \rightarrow Y$ and the second step is $C2 : Y \rightarrow X$. The multiplet's vev at point Y is unconstrained, since the ρ parameter measures at point X in today's universe, where the multiplet's vev equal to zero. Thus, the sphaleron energy at point Y can reach a sizable value. Parallel to the one-step EWPT analysis, we show the field's profile function solution in the right part of Figure 4 under the same value of λ_{13} and λ_s but a larger choice of v_ϕ . For a model parameter scan, the sphaleron energy at Y is presented in Figure 6.

In Figure 6, the intersection between the orange region and the right hand side of the vertical dashed λ_{13} line represents the unconstrained sphaleron energy domain. From eq. (53), we observe that the portal effective coupling λ_{13} doesn't affect the potential term V_{Two} under the $v = 0$ scenario at point Y , so that λ_{13} doesn't alter the sphaleron energy at Y . While, the greater value of λ_s , the higher value of the sphaleron energy. Therefore, the sphaleron energy's relationship with λ_{13} and λ_s at two-step EWPT differs from one-step ones. This difference can be deduced from the different sphaleron potential configuration in one-step eq. (46) and two-step eq. (53).

It is interesting to observe that there is a sizeable or-

ange region with sphaleron energy greater than the SM value. If this pattern persists at $T > 0$; if our universe undergoes a first order EWPT during the first step (C1); and if there exists sufficient BSM CPV to create the baryon asymmetry, this asymmetry can be well preserved at point Y. For demonstration in the real triplet extension, see Refs. [19–21, 49]. In general, the second step C2 to the Higgs phase could either preserve or erase this baryon asymmetry. If the second step is first order and if the sphaleron energy at point X is sufficiently large, then this asymmetry can be preserved in the final Higgs phase. A complete analysis of this possibility for the $T > 0$ general electroweak multiplet case will appear in a future study.

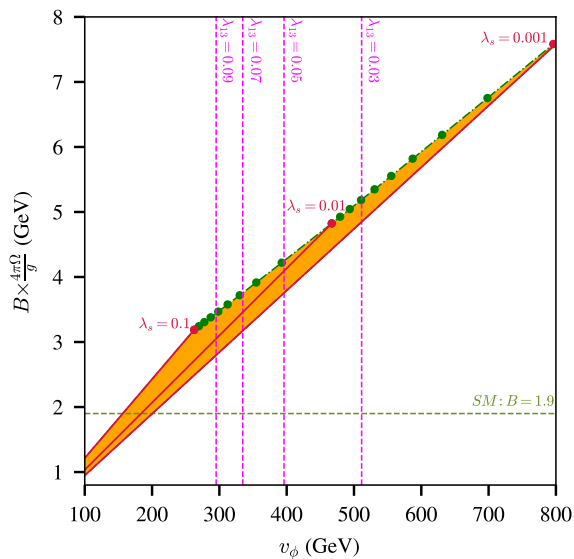


Figure 6: Sphaleron energy in the first step (point Y) of two-step EWPT. The bottom olive drab dashed line denotes the SM sphaleron B value, which is approximately equal to 1.9. The orange region represents the sphaleron energy under a feasible choice of v_ϕ and λ_s . The bottom red line represents $\lambda_s = 0.001$, while the upper red line denotes $\lambda_s = 0.1$, and λ_s continuously increase anticlockwise. The red or green dots represent the truncated points limited by the v_ϕ in eq. (56). The constraint from λ_{13} in eq. (58) rejects the left hand side of the vertical λ_{13} line. Therefore, the intersection of the orange region and right hand side of the dashed vertical λ_{13} line represents the viable sphaleron energy region.

Finally, we comment on model constraints implied by dark matter phenomenology. The work [37] researches such constraint, wherein the effective Higgs-septuplet portal coupling λ_{eff} should be very small in order to satisfy present direct detection limits. In our work, the effective portal parameter $\lambda_{13} = \lambda_{\text{eff}}/2$. In our parameter scan, we take λ_{13} smaller than 0.1 both in Figure 5 and Figure 6. We can verify that our parameter choice is unlimited under the newest dark matter direct search constraint [50].

V. CONCLUSION

Determining the origin of the cosmic baryon asymmetry remains an important research challenge at the interface of particle and nuclear physics with cosmology. Among various possible baryogenesis mechanisms, we focus on electroweak baryogenesis, which naturally connects with the Higgs mechanism. While the nature of EWSB and strength of CP-violation in the SM do not admit for successful EWBG, it can occur in a variety of BSM scenarios. Of particular interest for our study is the occurrence of a first order electroweak phase transition and the computation of the corresponding broken phase sphaleron rate. We make a detailed study of the sphaleron formalism and compute the sphaleron energy under different EWPT scenarios. For concreteness we have focused on an extension of the SM scalar sector with an electroweak septuplet, whose neutral component can contribute to the dark matter relic density.

For the sphaleron formalism, we summarize different sphaleron configurations that have been established by Manton and Klinkhamer (MK), Klinkhamer and Laterveer (KL), et.al. Further more, we show that MK and KL configurations are equivalent up to a unitary transformation. In the SU(2) multiplet extension to the SM, a proof of 1-form F_a invariance with respect to representation dimension is of crucial importance, which is based on the construction of high SU(2) sphaleron transformation matrix. Previously, Ahriche et al. analyse the sphaleron under SU(2) multiplet situation but without giving a proof of F_a invariance. In this work, we establish the general dimensional SU(2) transformation matrix and demonstrate the invariance property F_a . Besides this, we discuss the restrictions arising in the presence of more than one scalar field multiplet; topology pertaining to higher dimensional (beyond doublet) multiplets; equation of motion and choice of boundary conditions. Our formal considerations are benefit for clarifying some points that appeared in previous literatures.

For the multiple steps EWPT, we analyse the multiplet extension model's parameter constraint in one-step EWPT to mixed phase and two-step EWPT scenario separately. In both scenarios, we have five input parameters, the Higgs and septuplet vev, the Higgs and septuplet effective self couplings, and the Higgs-septuplet effective portal coupling. In one-step EWPT to mixed phase scenario, constrained by the ρ parameter, the additional multiplet's vev cannot be too large and its effect to the SM sphaleron energy is negligible. On the other hand, for two-step EWPT, the multiplet's vev at the end of first step is unconstrained, therefore can lead to a large enhancement of the sphaleron energy. If our universe undergoes a first order EWPT during the first step, then the baryon asymmetry can be well preserved during the first step of two-step EWPT.

In the future, numerous studies can be conducted based on this work. For instance, the computation of sphaleron energy under thermal corrections and the com-

putation of one-step EWPT with the Georgi-Machacek model, et.al.

Acknowledgments

M.J. Ramsey-Musolf, Y. Wu, and W. Zhang were supported in part by the National Natural Science Foundation of China under grant no. 11975150 and by the Ministry of Science and Technology of China under grant no. WQ20183100522. M. J. Ramsey-Musolf also gratefully acknowledges support under the Double First Class Plan of the Shanghai Jiao Tong University and sponsorship from Shanghai Tang Junyuan Education Foundation.

Appendix A: Other sphaleron configurations

1. AKY configuration

Under the general spherically symmetric ansatz, the gauge field configurations is written as [25]

$$A_j^a(x) = \frac{1}{g} [D(r)\epsilon_{jam}x_m + B(r)(r^2\delta_{ja} - x_jx_a) + C(r)x_jx_a], \quad (\text{A1})$$

The Higgs field is written as

$$H(x) = \frac{v}{\sqrt{2}} \left[H(r) + iK(r)\frac{\vec{\sigma} \cdot \vec{\hat{r}}}{2} \right] \begin{pmatrix} 0 \\ 1 \end{pmatrix}. \quad (\text{A2})$$

where $D(r), B(r), C(r), H(r)$ and $K(r)$ are all radial functions. Usually, the radial gauge condition sets $C(r) = 0$.

2. KKB configuration

Start form a set of orthonormal vectors [27]

$$\begin{aligned} \mathbf{u}_1(\phi) &= (\cos \phi, \sin \phi, 0), \\ \mathbf{u}_2(\phi) &= (0, 0, 1), \\ \mathbf{u}_3(\phi) &= (\sin \phi, -\cos \phi, 0), \end{aligned} \quad (\text{A3})$$

The fields are expanded as follows

$$\begin{aligned} A_i^a(\mathbf{r}) &= u_j^i(\phi)u_k^a(\phi)w_j^k(\rho, z), \\ a_i(\mathbf{r}) &= u_j^i(\phi)a_j(\rho, z), \\ H(\mathbf{r}) &= \tau^i u_j^i(\phi)h_j(\rho, z)\frac{v}{\sqrt{2}} \begin{pmatrix} 0 \\ 1 \end{pmatrix}. \end{aligned} \quad (\text{A4})$$

where we change the field labels to make them consistent with this study's convention.

Appendix B: Sphaleron Energy Computation

In this appendix, we provide detailed calculations of the sphaleron energy for the Yang-Mills term and the kinetic term in a general SU(2) multiplet dimension representation.

1. Yang-Mills term

We consider the SU(2) Yang-Mills term computation under a general representation.

$$\begin{aligned} F^{aij}F_{ij}^a &= F^{aij}F_{ij}^b \frac{1}{2S(R)} \text{Tr}[\{T^a, T^b\}] \\ &= \frac{1}{S(R)} \text{Tr}[\{F^{aij}T^a \cdot F_{ij}^b T^b\}], \end{aligned} \quad (\text{B1})$$

where $S(R)$ is the Dynkin index, and we use $\text{Tr}[\{T^a, T^b\}] = 2S(R)\delta^{ab}$. Since

$$F_{ij}^a T^a = \partial_i A_j^a T^a - \partial_j A_i^a T^a + g\epsilon^{abc} A_i^b A_j^c T^a, \quad (\text{B2})$$

and

$$\begin{aligned} \epsilon^{abc} A_i^b A_j^c T^a &= \epsilon^{bca} T^a A_i^b A_j^c, \\ &= \frac{1}{i} [T^b, T^c] A_i^b A_j^c, \\ &= \frac{1}{i} [A_i^b T^b A_j^c T^c - A_j^c T^c A_i^b T^b]. \end{aligned} \quad (\text{B3})$$

where we have used the fact that $[T^b, T^c] = i\epsilon^{bca} T^a$ for all SU(2) multiplet. We can deduce that the Yang-Mills

term is invariant for different SU(2) multiplet representations.

2. Kinetic term

For a general SU(2) multiplet, it's covariant derivative reads

$$(D_i \Phi) = \partial_i \Phi - ig A_i^a J^a \Phi - ig' a_i X \Phi, \quad (\text{B4})$$

Since our sphaleron construction occurs in spherical coordinates, the index $i \in [r, \theta, \phi]$. The kinetic term in the second phase of KL sphaleron configuration reads

$$\begin{aligned} (D_i \Phi)^\dagger (D_i \Phi) &= (\partial_i \Phi)^\dagger (\partial_i \Phi) + g^2 \langle \Phi^\dagger | J^b J^a | \Phi \rangle A_i^a A_i^b + g'^2 \langle \Phi^\dagger | X^2 | \Phi \rangle a^i a^i + 2gg' A_i^3 a_i J^3 X \Phi^\dagger \Phi, \\ &= (\partial_i \Phi)^\dagger (\partial_i \Phi) + h^2 g^2 \left[\frac{v^2}{4} (J(J+1) - (J^3)^2) A_\mu^+ A^{\mu-} + \frac{v^2}{2} (J^3)^2 A_\mu^3 A^{\mu 3} \right] \\ &\quad + g'^2 (J^3)^2 h^2 \frac{v^2}{2} (a_r^2 + a_\theta^2 + a_\phi^2) - gg' (J^3)^2 v^2 h^2 \left(\frac{a_\theta A_\theta^3}{r^2} + \frac{a_\phi A_\phi^3}{(r \sin(\theta))^2} \right), \end{aligned} \quad (\text{B5})$$

where

$$\begin{aligned} A_\mu^+ A^{\mu-} &= \frac{(A_\theta^1)^2 + (A_\theta^2)^2}{r^2} + \frac{(A_\phi^1)^2 + (A_\phi^2)^2}{r^2 \text{Sin}^2[\theta]}, \\ A_\mu^3 A^{\mu 3} &= \frac{(A_\theta^3)^2}{r^2} + \frac{(A_\phi^3)^2}{r^2 \text{Sin}^2[\theta]}. \end{aligned} \quad (\text{B6})$$

where we need to know the explicit expression of A_i^a , with $i \in [r, \theta, \phi]$ being the spherical coordinates label

and $a \in [1, 2, 3]$ being the SU(2) generators label. The expressions of A_i^a can be computed through eq. (7).

3. General energy form

The U(1) field sphaleron energy computation is straightforward, so we don't list the result here. Finally, we scale the sphaleron energy in following way [47]:

$$\int d^3x \left(\frac{1}{4} F_{ij}^a F_{ij}^a + \frac{1}{4} f_{ij} f_{ij} + (D_i \Phi)^\dagger (D_i \Phi) \right) \rightarrow \frac{4\pi\Omega}{g} \int d\xi \left(\frac{1}{4} F_{ij}^a F_{ij}^a(\xi) + \frac{1}{4} f_{ij} f_{ij}(\xi) + (D_i \Phi)^\dagger (D_i \Phi)(\xi) \right), \quad (\text{B7})$$

where we add the dimensionless radial parameter (ξ) to each component to label the differences before and after

the transformation. When $\mu = \frac{\pi}{2}$, the formal expression reads

$$\begin{aligned} \frac{1}{4} F_{ij}^a F_{ij}^a(\xi, \mu = \frac{\pi}{2}) &= \sin^2 \mu \left(\frac{8}{3} f'^2 + \frac{4}{3} f_3'^2 \right) + \frac{8}{\xi^2} \sin^4 \mu \left\{ \frac{2}{3} f_3^2 (1-f)^2 + \frac{1}{3} \{f(2-f) - f_3\}^2 \right\}, \\ \frac{1}{4} f_{ij} f_{ij}(\xi, \mu = \frac{\pi}{2}) &= \frac{4}{3} \left(\frac{g}{g'} \right)^2 \left\{ \sin^2 \mu f_0'^2 + \frac{2}{\xi^2} \sin^4 \mu (1-f_0)^2 \right\}, \\ (D_i \Phi)^\dagger (D_i \Phi)(\xi, \mu = \frac{\pi}{2}) &= \frac{v_2^2}{\Omega^2} \left\{ \frac{1}{2} \xi^2 \phi'^2 + \frac{4}{3} \sin^2 \mu \phi^2 \left\{ (J(J+1) - J_3^2) (1-f)^2 + J_3^2 (f_0 - f_3)^2 \right\} \right\}. \end{aligned} \quad (\text{B8})$$

Appendix C: Mass Matrices in the SU(2) doublet plus septuplet model

In this appendix, we list the explicit mass matrices that appear in eq. (44).

1. Higgs Matrix

$$H_{2 \times 2} = \begin{pmatrix} 2\lambda v^2 & 2\lambda_{13} v v_\phi \\ 2\lambda_{13} v v_\phi & 2v_\phi^2 \lambda_s \end{pmatrix}. \quad (C1)$$

where λ_{13} and λ_s are two combined parameters that defined in equations eq. (42) and eq. (43).

2. Pseudo-Scalar Matrix

$$Pi_{2 \times 2} = \begin{pmatrix} 0 & 0 \\ 0 & \frac{4\text{Re}(M_B^2)}{\sqrt{7}} + v_\phi^2 \kappa_\pi + \frac{2\text{Re}(\lambda_3)v^2}{\sqrt{14}} \end{pmatrix}, \quad (C2)$$

where

$$\kappa_\pi = \frac{2}{7}[\text{Re}(\kappa_0'') - 4\text{Re}(\kappa_0')] + \frac{8}{21\sqrt{5}}[\text{Re}(\kappa_2'') - 4\text{Re}(\kappa_2')]. \quad (C3)$$

3. Charged Higgs Matrices

$$C1_{3 \times 3} = \begin{pmatrix} 0 & -\frac{v v_\phi \lambda_2}{2\sqrt{14}} & -\frac{v v_\phi \lambda_2}{2\sqrt{14}} \\ -\frac{v v_\phi \lambda_2}{2\sqrt{14}} & M_A^2 + v_\phi^2 \kappa_{122} + v^2 \left(\frac{\lambda_1}{2} + \frac{\lambda_2}{4\sqrt{42}} \right) & \frac{2\text{Re}(M_B^2)}{\sqrt{7}} + \frac{\text{Re}(\lambda_3)v^2}{\sqrt{14}} - v_\phi^2 \kappa_{123} \\ -\frac{v v_\phi \lambda_2}{2\sqrt{14}} & \frac{2\text{Re}(M_B^2)}{\sqrt{7}} + \frac{\text{Re}(\lambda_3)v^2}{\sqrt{14}} - v_\phi^2 \kappa_{123} & M_A^2 + v_\phi^2 \kappa_{122} + v^2 \left(\frac{\lambda_1}{2} - \frac{\lambda_2}{4\sqrt{42}} \right) \end{pmatrix}, \quad (C4)$$

where

$$\begin{aligned} \kappa_{122} &= \frac{\kappa_2 - 4\text{Re}(\kappa_2'')}{21\sqrt{5}} - \frac{\text{Re}(\kappa_0'')}{7}, \\ \kappa_{123} &= \frac{1}{7}(\kappa_0 + 2\text{Re}(\kappa_0') - \text{Re}(\kappa_0'')) + \frac{1}{21\sqrt{5}}(3\kappa_2 + 8\text{Re}(\kappa_2') - 4\text{Re}(\kappa_2'')). \end{aligned} \quad (C5)$$

The three eigenvalues of matrix $C1_{3 \times 3}$ are difficult to obtain. However, we can numerically calculate them, and we find that one of these eigenvalues equal to zero. This zero eigenvalue correspond to the massless charged Higgs particle.

$$C2_{2 \times 2} = \begin{pmatrix} M_A^2 + v_\phi^2 \kappa_{211} + v^2 \left(\frac{\lambda_1}{2} + \frac{\lambda_2}{2\sqrt{42}} \right) & -\frac{2\text{Re}(M_B^2)}{\sqrt{7}} - \frac{\text{Re}(\lambda_3)v^2}{\sqrt{14}} + v_\phi^2 \kappa_{212} \\ -\frac{2\text{Re}(M_B^2)}{\sqrt{7}} - \frac{\text{Re}(\lambda_3)v^2}{\sqrt{14}} + v_\phi^2 \kappa_{212}^* & M_A^2 + v_\phi^2 \kappa_{211} + v^2 \left(\frac{\lambda_1}{2} - \frac{\lambda_2}{2\sqrt{42}} \right) \end{pmatrix}, \quad (C6)$$

where

$$\begin{aligned} \kappa_{211} &= \frac{2\sqrt{5}}{21}[\kappa_2 - \text{Re}(\kappa_2'')] - \frac{\text{Re}(\kappa_0'')}{7}, \\ \kappa_{212} &= \frac{1}{7}(\kappa_0 + 2\kappa_0' - \kappa_0'') + \frac{2\sqrt{5}}{21}(2\kappa_2' - \kappa_2''). \end{aligned} \quad (C7)$$

$$C_{32 \times 2} = \begin{pmatrix} M_A^2 + v_\phi^2 \kappa_{311} + v^2 \left(\frac{\lambda_1}{2} + \frac{1}{4} \sqrt{\frac{3}{14}} \lambda_2 \right) & \frac{2\text{Re}(M_B^2)}{\sqrt{7}} + \frac{\text{Re}(\lambda_3)v^2}{\sqrt{14}} + v_\phi^2 \kappa_{312} \\ \frac{2\text{Re}(M_B^2)}{\sqrt{7}} + \frac{\text{Re}(\lambda_3)v^2}{\sqrt{14}} + v_\phi^2 \kappa_{312}^* & M_A^2 + v_\phi^2 \kappa_{311} + v^2 \left(\frac{\lambda_1}{2} - \frac{1}{4} \sqrt{\frac{3}{14}} \lambda_2 \right) \end{pmatrix}, \quad (\text{C8})$$

where

$$\begin{aligned} \kappa_{c311} &= -\frac{\text{Re}(\kappa_0'')}{7} + \frac{\sqrt{5}\text{Re}(\kappa_2'')}{21}, \\ \kappa_{c312} &= -\frac{1}{7}(\kappa_0 + 2\kappa_0' - \kappa_0'') + \frac{\sqrt{5}}{21}(\kappa_2 + 2\kappa_2' - \kappa_2''). \end{aligned} \quad (\text{C9})$$

-
- [1] A. D. Sakharov, *Pisma Zh. Eksp. Teor. Fiz.* **5**, 32 (1967).
[2] M. B. Gavela, P. Hernandez, J. Orloff, and O. Pene, *Mod. Phys. Lett. A* **9**, 795 (1994), hep-ph/9312215.
[3] P. Huet and E. Sather, *Phys. Rev. D* **51**, 379 (1995), hep-ph/9404302.
[4] M. B. Gavela, P. Hernandez, J. Orloff, O. Pene, and C. Quimbay, *Nucl. Phys. B* **430**, 382 (1994), hep-ph/9406289.
[5] K. Kajantie, M. Laine, K. Rummukainen, and M. E. Shaposhnikov, *Phys. Rev. Lett.* **77**, 2887 (1996), hep-ph/9605288.
[6] M. Gurtler, E.-M. Ilgenfritz, and A. Schiller, *Phys. Rev. D* **56**, 3888 (1997), hep-lat/9704013.
[7] M. Laine and K. Rummukainen, *Nucl. Phys. B Proc. Suppl.* **73**, 180 (1999), hep-lat/9809045.
[8] F. Csikor, Z. Fodor, and J. Heitger, *Phys. Rev. Lett.* **82**, 21 (1999), hep-ph/9809291.
[9] Y. Aoki, F. Csikor, Z. Fodor, and A. Ukawa, *Phys. Rev. D* **60**, 013001 (1999), hep-lat/9901021.
[10] D. E. Morrissey and M. J. Ramsey-Musolf, *New J. Phys.* **14**, 125003 (2012), 1206.2942.
[11] M. J. Ramsey-Musolf, *JHEP* **09**, 179 (2020), 1912.07189.
[12] V. A. Kuzmin, V. A. Rubakov, and M. E. Shaposhnikov, *Phys. Lett. B* **155**, 36 (1985).
[13] V. A. Rubakov and M. E. Shaposhnikov, *Usp. Fiz. Nauk* **166**, 493 (1996), hep-ph/9603208.
[14] H. H. Patel and M. J. Ramsey-Musolf, *JHEP* **07**, 029 (2011), 1101.4665.
[15] P. B. Arnold and L. D. McLerran, *Phys. Rev. D* **36**, 581 (1987).
[16] L. Carson, X. Li, L. D. McLerran, and R.-T. Wang, *Phys. Rev. D* **42**, 2127 (1990).
[17] J. Baacke and S. Junker, *Phys. Rev. D* **49**, 2055 (1994), hep-ph/9308310.
[18] H. Georgi and M. Machacek, *Nucl. Phys. B* **262**, 463 (1985).
[19] H. H. Patel and M. J. Ramsey-Musolf, *Phys. Rev. D* **88**, 035013 (2013), 1212.5652.
[20] N. Blinov, J. Kozaczuk, D. E. Morrissey, and C. Tamarit, *Phys. Rev. D* **92**, 035012 (2015), 1504.05195.
[21] L. Niemi, M. J. Ramsey-Musolf, T. V. I. Tenkanen, and D. J. Weir, *Phys. Rev. Lett.* **126**, 171802 (2021), 2005.11332.
[22] N. S. Manton, *Phys. Rev. D* **28**, 2019 (1983).
[23] F. R. Klinkhamer and N. S. Manton, *Phys. Rev. D* **30**, 2212 (1984).
[24] F. R. Klinkhamer and R. Laterveer, *Z. Phys. C* **53**, 247 (1992).
[25] T. Akiba, H. Kikuchi, and T. Yanagida, *Phys. Rev. D* **38**, 1937 (1988).
[26] C. Rebbi and P. Rossi, *Phys. Rev. D* **22**, 2010 (1980).
[27] B. Kleihaus, J. Kunz, and Y. Brihaye, *Phys. Lett. B* **273**, 100 (1991).
[28] S. H. H. Tye and S. S. C. Wong, *Phys. Rev. D* **92**, 045005 (2015), 1505.03690.
[29] A. Ahriche, T. A. Chowdhury, and S. Nasri, *JHEP* **11**, 096 (2014), 1409.4086.
[30] R. M. Fonseca, *Comput. Phys. Commun.* **267**, 108085 (2021), 2011.01764.
[31] S. Inoue, M. J. Ramsey-Musolf, and Y. Zhang, *Phys. Rev. D* **89**, 115023 (2014), 1403.4257.
[32] E. Witten, *Phys. Rev. Lett.* **38**, 121 (1977).
[33] R. Jackiw and S.-Y. Pi, *Phys. Rev. D* **61**, 105015 (2000), hep-th/9911072.
[34] S. S. AbdusSalam and T. A. Chowdhury, *JCAP* **05**, 026 (2014), 1310.8152.
[35] K. Hally, H. E. Logan, and T. Pilkington, *Phys. Rev. D* **85**, 095017 (2012), 1202.5073.
[36] K. Earl, K. Hartling, H. E. Logan, and T. Pilkington, *Phys. Rev. D* **88**, 015002 (2013), 1303.1244.
[37] W. Chao, G.-J. Ding, X.-G. He, and M. Ramsey-Musolf, *JHEP* **08**, 058 (2019), 1812.07829.
[38] M. Cirelli, N. Fornengo, and A. Strumia, *Nucl. Phys. B* **753**, 178 (2006), hep-ph/0512090.
[39] K. Kajantie, M. Laine, K. Rummukainen, and M. E. Shaposhnikov, *Nucl. Phys. B* **458**, 90 (1996), hep-ph/9508379.
[40] E. Braaten and A. Nieto, *Phys. Rev. D* **51**, 6990 (1995), hep-ph/9501375.
[41] K. Farakos, K. Kajantie, K. Rummukainen, and M. E. Shaposhnikov, *Nucl. Phys. B* **425**, 67 (1994), hep-ph/9404201.
[42] J. Löfgren, M. J. Ramsey-Musolf, P. Schicho, and T. V. I. Tenkanen, (2021), 2112.05472.
[43] J. Hirvonen, J. Löfgren, M. J. Ramsey-Musolf, P. Schicho, and T. V. I. Tenkanen, *JHEP* **07**, 135 (2022), 2112.08912.
[44] W. J. G. de Blok, *Adv. Astron.* **2010**, 789293 (2010), 0910.3538.
[45] S. Tulin and H.-B. Yu, *Phys. Rept.* **730**, 1 (2018),

- 1705.02358.
- [46] Q.-H. Cao, K. Hashino, X.-X. Li, and J.-H. Yue, (2022), 2212.07756.
- [47] M. Quiros, Finite temperature field theory and phase transitions, in *ICTP Summer School in High-Energy Physics and Cosmology*, pp. 187–259, 1999, hep-ph/9901312.
- [48] Particle Data Group, R. L. Workman *et al.*, PTEP **2022**, 083C01 (2022).
- [49] S. Inoue, G. Ovanesyan, and M. J. Ramsey-Musolf, Phys. Rev. D **93**, 015013 (2016), 1508.05404.
- [50] LZ, J. Aalbers *et al.*, (2022), 2207.03764.